


Dyakonov waves in biaxial anisotropic crystals

Evgenii E. Narimanov

School of Electrical and Computer Engineering and Birck Nanotechnology Center, Purdue University, West Lafayette, Indiana 47907, USA

 (Received 30 May 2018; published 11 July 2018)

We present the general analytical theory for Dyakonov surface waves at the interface of a biaxial anisotropic dielectric with an isotropic medium. We demonstrate that these surface waves can be divided into two distinct classes, with qualitatively different spatial behavior. We obtain explicit expressions for the Dyakonov waves' dispersion and the parameter ranges for their existence.

DOI: [10.1103/PhysRevA.98.013818](https://doi.org/10.1103/PhysRevA.98.013818)

I. INTRODUCTION

Electromagnetic surface waves, strongly localized near the interface of two different media, play an important role in many areas of science and technology—from optical microscopy [1] and biosensing [2] to nano-optical tweezing [3] and photonic integrated circuits [4]. Electromagnetic surface waves are responsible for such phenomena as superlensing [5,6], enhanced Raman scattering [7,8], and extraordinary light transmission through subwavelength holes [9]. While there exists a number of different kinds of surface electromagnetic waves, such as e.g., surface plasmons at the interface of a metal and a dielectric [10] or Tamm-Shockley states [11–13] at the boundary of a photonic crystal [14–16], a new class of surface electromagnetic modes has recently gained considerable attention [17–23]. These Dyakonov surface waves exist at the interface of an isotropic and anisotropic dielectric media. They can be supported by transparent optical materials and thus do not suffer from the metallic absorption that plagues surface plasmons [24]. Compared to the Tamm-Shockley state, a Dyakonov wave does not require any periodic patterning of the material forming the system, with the resulting light scattering due to the inevitable disorder as a result of an imperfect fabrication of such lattice.

The presence of Dyakonov waves at the isotropic-anisotropic interface has been firmly established in the experiment [23] and a number of adequate theoretical methods exists for their quantitative description [18,19,21]. However, due to the inevitable complexity of the boundary conditions at the interface of a fully anisotropic dielectric, the resulting theoretical description generally leads to a system of nonlinear equations that must be solved numerically. While this may be considered a straightforward task, Dyakonov waves are usually extended over many wavelengths [21] and are therefore close to the propagation wave threshold—which makes the numerical solution more challenging. What is even more important, with the theoretical “toolbox” limited to numerical methods, the root-finding algorithm may even miss an entire class of possible solutions.

In this work, we present a complete analytical solution for the Dyakonov surface waves at the interface of an isotropic and a biaxial dielectric medium. We show that, depending on the magnitudes of the dielectric permittivity components in the system, the interface can simultaneously support two different

classes of surface waves, with qualitatively different spatial behavior.

II. MODEL

We consider the interface of an isotropic dielectric with the permittivity ϵ_0 , with a biaxial anisotropic medium, with the permittivity tensor

$$\epsilon = \begin{pmatrix} \epsilon_x & 0 & 0 \\ 0 & \epsilon_y & 0 \\ 0 & 0 & \epsilon_z \end{pmatrix}. \quad (1)$$

We furthermore assume that one of the symmetry directions of the anisotropic crystal (which will be referred to as the axis z in our coordinate system—see Fig. 1) is normal to the surface, as this is generally the case for a high-quality interface. While a nonorthogonal orientation of $\hat{\mathbf{z}}$ with respect to the plane of surface is possible, this would lead to a relatively high density of surface defects—thus making the theory for surface waves at an ideal planar interface irrelevant for most practical applications. For convenience, the coordinate system origin $z = 0$ is chosen at the plane of the interface—see Fig. 1.

In this work, we focus on guided surface waves with the in-plane momentum $\mathbf{q} \equiv (q_x, q_y)$,

$$\mathbf{E}(\mathbf{r}, t) = \mathbf{E}_{\mathbf{q}}(z) \exp(iq_x x + iq_y y - i\omega t), \quad (2)$$

$$\mathbf{B}(\mathbf{r}, t) = \mathbf{B}_{\mathbf{q}}(z) \exp(iq_x x + iq_y y - i\omega t), \quad (3)$$

where

$$E_{\mathbf{q}}(|z| \rightarrow \infty) \rightarrow 0, \quad B_{\mathbf{q}}(|z| \rightarrow \infty) \rightarrow 0. \quad (4)$$

III. ELECTROMAGNETIC WAVES IN A BIAXIAL MEDIUM

For an evanescent wave that decays away from the $z = 0$ interface, we have

$$\mathbf{E}_{\mathbf{q}}(z) = \mathbf{e} \cdot \exp(-\kappa z), \quad (5)$$

$$\mathbf{B}_{\mathbf{q}}(z) = \mathbf{b} \cdot \exp(-\kappa z). \quad (6)$$

Note that, for a complex κ , the expressions (5) and (6) also describe the propagating waves in the medium.

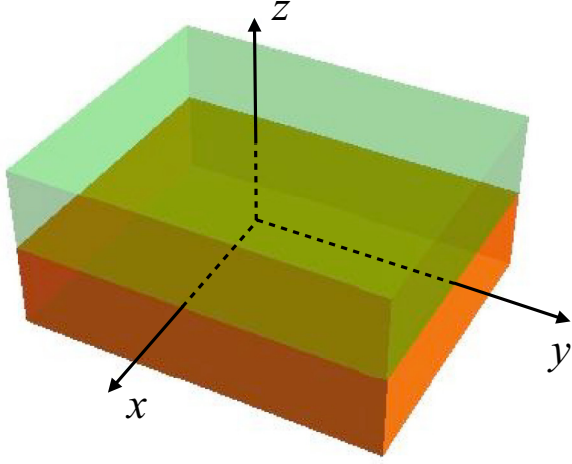


FIG. 1. Schematics of the coordinate system at the planar interface of a transparent isotropic medium (orange, bottom) and biaxial anisotropic dielectric (green area, top).

Substituting (2) and (3) with (5) and (6) into Maxwell's equations, we obtain

$$b_x = \frac{c}{\omega}(q_y e_z - i\kappa e_y), \quad (7)$$

$$b_y = \frac{c}{\omega}(i\kappa e_x - q_x e_z), \quad (8)$$

$$b_z = \frac{c}{\omega}(q_x e_y - q_y e_x), \quad (9)$$

and

$$\mathcal{M} \begin{pmatrix} e_x \\ e_y \\ e_z \end{pmatrix} = 0, \quad (10)$$

where

$$\mathcal{M} \equiv \begin{pmatrix} \Delta_x(\kappa) & q_x q_y & i\kappa q_x \\ q_x q_y & \Delta_y(\kappa) & i\kappa q_y \\ i\kappa q_x & i\kappa q_y & \Delta_z(\kappa) \end{pmatrix}, \quad (11)$$

and

$$\Delta_x(\kappa) = \epsilon_x \left(\frac{\omega}{c} \right)^2 - q_y^2 + \kappa^2, \quad (12)$$

$$\Delta_y(\kappa) = \epsilon_y \left(\frac{\omega}{c} \right)^2 - q_x^2 + \kappa^2, \quad (13)$$

$$\Delta_z(\kappa) = \epsilon_z \left(\frac{\omega}{c} \right)^2 - q_x^2 - q_y^2. \quad (14)$$

From (10) we find the electrical field components in terms of the amplitude a ,

$$e_x = i\kappa q_x (q_y^2 - \Delta_y(\kappa))a, \quad (15)$$

$$e_y = i\kappa q_y (q_x^2 - \Delta_x(\kappa))a, \quad (16)$$

$$e_z = (\Delta_x(\kappa) \cdot \Delta_y(\kappa) - q_x^2 q_y^2)a, \quad (17)$$

which together with (7)–(9) define the entire electromagnetic field (\mathbf{e} , \mathbf{b}) in (5) and (6).

Also, from Eq. (10) we obtain

$$\det[\mathcal{M}] = 0, \quad (18)$$

which yields

$$\begin{aligned} \epsilon_z \kappa^4 + \left[\epsilon_z (\epsilon_x + \epsilon_y) \left(\frac{\omega}{c} \right)^2 - (\epsilon_x + \epsilon_z) q_x^2 \right. \\ \left. - (\epsilon_y + \epsilon_z) q_y^2 \right] \kappa^2 + \left[\epsilon_z \left(\frac{\omega}{c} \right)^2 - q_x^2 - q_y^2 \right] \\ \times \left[\epsilon_x \epsilon_y \left(\frac{\omega}{c} \right)^2 - \epsilon_x q_x^2 - \epsilon_y q_y^2 \right] = 0. \end{aligned} \quad (19)$$

Equation (19) is a quadratic equation for κ^2 , with the straightforward solution

$$\kappa_{\pm}^2 = \frac{1}{2} \left\{ \frac{\epsilon_x + \epsilon_z}{\epsilon_z} q_x^2 + \frac{\epsilon_y + \epsilon_z}{\epsilon_z} q_y^2 - (\epsilon_x + \epsilon_y) \left(\frac{\omega}{c} \right)^2 \pm \sqrt{D} \right\}, \quad (20)$$

where the discriminant

$$\begin{aligned} D = \left[(\epsilon_x - \epsilon_y) \left(\frac{\omega}{c} \right)^2 + \frac{\epsilon_z - \epsilon_x}{\epsilon_z} q_x^2 + \frac{\epsilon_y - \epsilon_z}{\epsilon_z} q_y^2 \right]^2 \\ + 4 \frac{(\epsilon_x - \epsilon_z)(\epsilon_y - \epsilon_z)}{\epsilon_z^2} q_x^2 q_y^2. \end{aligned} \quad (21)$$

When the discriminant is positive, there are three distinct possibilities for the nature of the waves supported by the anisotropic dielectric. If the right-hand side of Eq. (20) is positive for κ_+^2 and κ_-^2 , both waves with the “in-plane” momentum $\mathbf{q} \equiv (q_x, q_y)$ are evanescent. In the opposite case, when the right-hand side of Eq. (20) is negative in both cases, the corresponding two waves are propagating. Finally, when it's positive for one choice of the sign in (20) and negative for the other, we find that for the given in-plane momentum \mathbf{q} the dielectric interface supports one propagating and one evanescent wave.

As follows from Eq. (21), the discriminant is positive-definite (for any \mathbf{q}) in each of the following cases: (i) any uniaxial dielectric ($\epsilon_x = \epsilon_y$ or $\epsilon_x = \epsilon_z$ or $\epsilon_y = \epsilon_z$), (ii) $\epsilon_z < \min[\epsilon_x, \epsilon_y]$, and (iii) $\epsilon_z > \max[\epsilon_x, \epsilon_y]$.

The boundaries that separate different portions of the (q_x, q_y) phase space that respectively support only the propagating waves, or only the evanescent fields, or a mixture of evanescent and propagating waves, are given by

$$q_x^2 + q_y^2 = \epsilon_z \left(\frac{\omega}{c} \right)^2 \quad (22)$$

and

$$\frac{q_x^2}{\epsilon_y} + \frac{q_y^2}{\epsilon_x} = \left(\frac{\omega}{c} \right)^2. \quad (23)$$

This behavior is illustrated in Fig. 2.

However, if

$$\min[\epsilon_x, \epsilon_y] < \epsilon_z < \max[\epsilon_x, \epsilon_y], \quad (24)$$

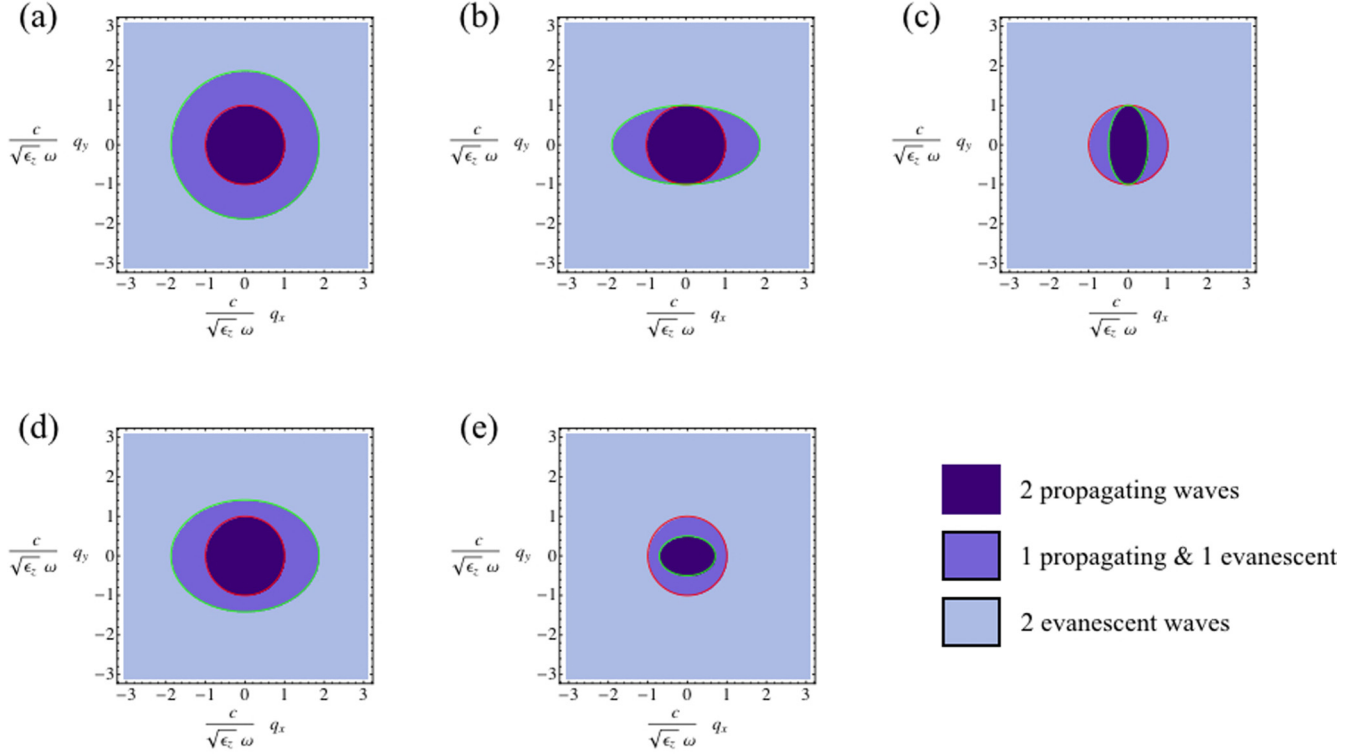


FIG. 2. “Phase space” for the waves with “in-plane” momentum \mathbf{q} [see Eqs. (5) and (6)] supported by an anisotropic dielectric. Panels (a), (b), and (c) correspond to a uniaxial dielectric, with $\epsilon_x = \epsilon_y > \epsilon_z$ (a), $\epsilon_x = \epsilon_z < \epsilon_y$ (b), and $\epsilon_x = \epsilon_z > \epsilon_y$ (c), respectively. Panels (d) and (e) represent the case of a biaxial dielectric, correspondingly with $\epsilon_z < \epsilon_x < \epsilon_y$ (d) and $\epsilon_x < \epsilon_y < \epsilon_z$ (e). The red line [the inner boundary in (a),(b),(d) and the outer boundary in (c),(e)] corresponds to Eq. (22) and the green line [the outer boundary in (a),(b),(d) and the inner boundary in (c),(e)] represents Eq. (23). The dielectric permittivity tensor components satisfy (a) $\epsilon_x = \epsilon_y = 3.5\epsilon_z$, (b) $\epsilon_x = \epsilon_z = 3.5\epsilon_y$, (c) $\epsilon_x = \epsilon_z = \epsilon_y/4$, (d) $\epsilon_x = 2\epsilon_z$ and $\epsilon_y = 3.5\epsilon_z$, (e) $\epsilon_x = \epsilon_z/4$, and $\epsilon_y = \epsilon_z/2$.

the discriminant in Eq. (21) can, and does, become negative for certain ranges of the values of q_x and q_y . In this case, κ_{\pm} is complex, with nonzero values for both its real and imaginary parts. These “ghost waves,” recently described in Ref. [25], combine the oscillatory behavior of the propagating waves with the exponential decay characteristic of the evanescent fields and represent the third class of the waves that can be supported by a transparent dielectric medium.

When the inequality (24) is satisfied, the boundaries of the portion of the (q_x, q_y) phase space of the ghost modes are defined by the four equations

$$\sqrt{\frac{|\epsilon_x - \epsilon_z|}{\epsilon_z}} q_x \pm \sqrt{\frac{|\epsilon_y - \epsilon_z|}{\epsilon_z}} q_y \pm \sqrt{|\epsilon_y - \epsilon_x|} \frac{\omega}{c} = 0. \quad (25)$$

Figure 3 shows the phase space of a biaxial anisotropic dielectric that supports ghost waves. Note its nontrivial structure near the point corresponding to the intersection of the boundaries described by Eqs. (22) and (23) in the magnified view of its panel (b).

When the permittivity ϵ_z in the normal-to-the-interface direction approaches the value of one of the in-plane permittivities ϵ_x or ϵ_y , the ghost regions in the phase space collapse to increasingly narrow strips parallel to either the q_x (when $\epsilon_z \rightarrow \epsilon_x$) or q_y (for $\epsilon_z \rightarrow \epsilon_y$) axis. This “collapse” is however relatively slow, and substantial ghost regions are still present

even when the permittivity is within 1% of the critical value, as seen in Fig. 4.

Most importantly, ghost regions have substantial presence in actual biaxial anisotropic crystals. This is illustrated in Fig. 5, where we show the phase space for the sodium nitrite NaNO_2 , with the dielectric permittivity tensor components [26] $\epsilon_x = 1.806$, $\epsilon_y = 2.726$, and $\epsilon_z = 1.991$.

While Eqs. (7)–(17) adequately describe the general case of a dielectric crystal with arbitrary degree of anisotropy, the isotropic limit $\epsilon_x \rightarrow \epsilon_y \rightarrow \epsilon_z \rightarrow \epsilon_0$ is singular, as here both κ_+ and κ_- are identical,

$$\kappa_+(\epsilon_x, \epsilon_y, \epsilon_z \rightarrow \epsilon_0) = \kappa_-(\epsilon_x, \epsilon_y, \epsilon_z \rightarrow \epsilon_0) = \kappa_0, \quad (26)$$

with

$$\kappa_0 = q_x^2 + q_y^2 - \epsilon_0 \left(\frac{\omega}{c} \right)^2, \quad (27)$$

and direct substitution of (26) and (27) into (15)–(17) and (7)–(9) yields

$$e_x, e_y, e_z, b_x, b_y, b_z \rightarrow 0a_0, \quad (28)$$

with $a_0 \rightarrow \infty$. This uncertainty can be removed if we explicitly introduce s and p polarizations, correspondingly with $e_z^{(s)} = 0$ and $b_z^{(p)} = 0$:

$$e_x^{(s)} = q_y a_s, \quad (29)$$

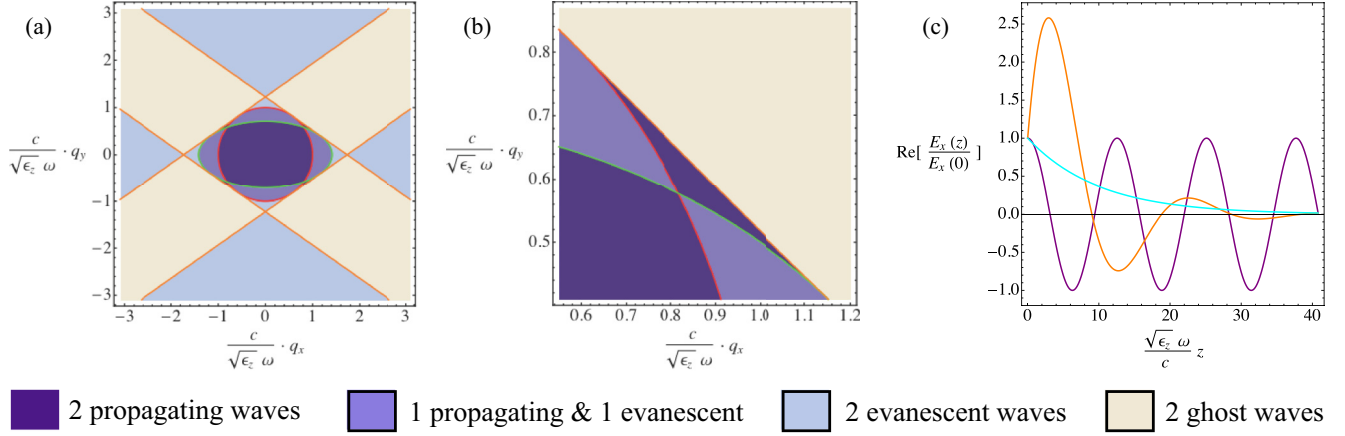


FIG. 3. Phase space for the waves with in-plane momentum \mathbf{q} [see Eqs. (5) and (6)], supported by a biaxial anisotropic dielectric with $\epsilon_x < \epsilon_z < \epsilon_y$. Note the presence of the ghost waves in the regions bounded by four orange (straight) lines defined by Eq. (25). As in Fig. 2, the red (gray) line corresponds to Eq. (22), and the green (light gray) line represents Eq. (23). Panels (a) and (b) show the “full” and the “magnified” view of the phase space. Panel (c) displays real-space field profiles for a propagating wave (oscillatory violet curve, calculated for $q_x = \sqrt{\epsilon_z} \omega/c$, $q_y = 0.5 \sqrt{\epsilon_z} \omega/c$), an evanescent wave (monotonic cyan curve, calculated for $q_x = 1.01 \sqrt{\epsilon_z} \omega/c$, $q_y = 0$), and a ghost wave (decaying oscillatory orange curve, calculated for $q_x = \sqrt{\epsilon_z} \omega/c$, $q_y = 0.525 \sqrt{\epsilon_z} \omega/c$). Here $\epsilon_x/\epsilon_z = 0.5$ and $\epsilon_y/\epsilon_z = 2$.

$$e_y^{(s)} = -q_x a_s, \quad (30)$$

$$e_z^{(s)} = 0, \quad (31)$$

$$b_x^{(s)} = \frac{ic\kappa_0}{\omega} q_x a_s, \quad (32)$$

$$b_y^{(s)} = \frac{ic\kappa_0}{\omega} q_y a_s, \quad (33)$$

$$b_z^{(s)} = -\frac{cq^2}{\omega} a_s, \quad (34)$$

Here

$$e_z^{(p)} = \frac{iq^2}{\kappa_0} a_p, \quad (37)$$

$$b_x^{(p)} = \frac{i\omega\epsilon_0}{c\kappa_0} q_y a_p, \quad (38)$$

$$b_y^{(p)} = -\frac{i\omega\epsilon_0}{c\kappa_0} q_x a_p, \quad (39)$$

$$b_z^{(p)} = 0. \quad (40)$$

and

$$e_x^{(p)} = q_x a_p, \quad (35)$$

$$e_y^{(p)} = q_y a_p, \quad (36)$$

$$q \equiv \sqrt{q_x^2 + q_y^2}, \quad (41)$$

while a_s and a_p are the scaled amplitudes of the s - and p -polarized waves, respectively.

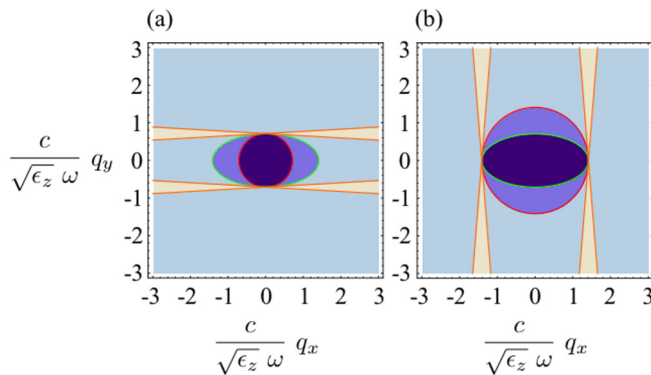


FIG. 4. Phase space for a biaxial anisotropic material for $\epsilon_z \rightarrow \epsilon_x$ (a) and $\epsilon_z \rightarrow \epsilon_y$ (b). In both cases $\epsilon_y/\epsilon_x = 4$, while the z component of the permittivity ϵ_z is such that $\epsilon_z/\epsilon_x = 1.01$ (a) and $\epsilon_z/\epsilon_y = 0.99525$ (b). The phase-space color code is the same as in Figs. 2 and 3. Note the presence of relatively large ghost regions even though ϵ_z in both cases is within 1% from its limiting values.

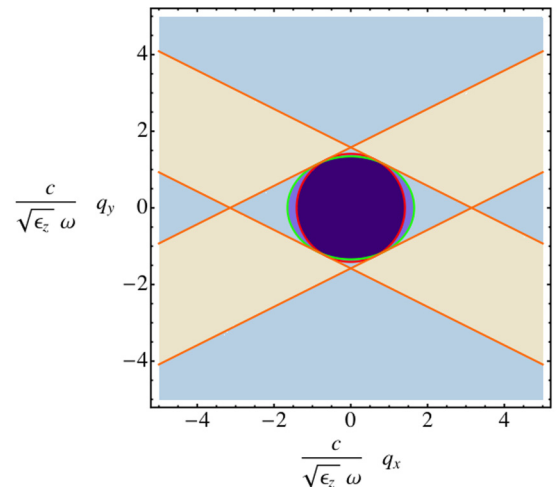


FIG. 5. Phase space for sodium nitrite, with $\epsilon_x = 1.806$, $\epsilon_y = 2.726$, and $\epsilon_z = 1.991$.

IV. DYAKONOV WAVE

Assuming that the interface at $z = 0$ separates the transparent isotropic medium with the permittivity ϵ_0 at $z < 0$ from biaxial anisotropic dielectric with the permittivity tensor (1), for the guided surface wave with the in-plane momentum $\mathbf{q} = (q_x, q_y)$ we obtain

$$\mathbf{E}_{\mathbf{q}}(z) = \begin{cases} (a_s \mathbf{e}_s + a_p \mathbf{e}_p) e^{\kappa_0 z}, & z < 0, \\ a_+ \mathbf{e}_+ e^{-\kappa_- z} + a_- \mathbf{e}_+ e^{-\kappa_- z}, & z > 0 \end{cases} \quad (42)$$

and

$$\mathbf{B}_{\mathbf{q}}(z) = \begin{cases} (a_s \mathbf{b}_s + a_p \mathbf{b}_p) e^{\kappa_0 z}, & z < 0, \\ b_+ \mathbf{e}_+ e^{-\kappa_- z} + b_- \mathbf{e}_+ e^{-\kappa_- z}, & z > 0, \end{cases} \quad (43)$$

where [note the sign change $\kappa_0 \rightarrow -\kappa_0$ from (29)–(40) to (44)–(47) as the evanescent field for $z < 0$ behaves as $\exp(+\kappa_0 z)$]

$$\mathbf{e}_s = (q_y, -q_x, 0), \quad (44)$$

$$\mathbf{b}_s = -\frac{c}{\omega} (i\kappa_0 q_x, i\kappa_0 q_y, q_x^2 + q_y^2), \quad (45)$$

$$\mathbf{e}_p = \left(q_x, q_y, -\frac{i}{\kappa_0} (q_x^2 + q_y^2) \right), \quad (46)$$

$$\mathbf{b}_p = \frac{i\omega\epsilon_0}{c\kappa_0} (-q_y, q_x, 0) \quad (47)$$

and

$$\mathbf{e}_{\pm} = (i\kappa_{\pm} q_x (q_y^2 - \Delta_y(\kappa_{\pm})), i\kappa_{\pm} q_y (q_x^2 - \Delta_x(\kappa_{\pm})), \Delta_x(\kappa_{\pm})\Delta_y(\kappa_{\pm}) - q_x^2 q_y^2), \quad (48)$$

$$\mathbf{b}_{\pm} = \frac{c}{\omega} (q_y (\epsilon_y \Delta_x(\kappa_{\pm}) - \epsilon_x q_x^2) - q_x (\epsilon_x \Delta_y(\kappa_{\pm}) - \epsilon_y q_y^2), i q_x q_y \kappa_{\pm} (\epsilon_y - \epsilon_x)). \quad (49)$$

With nonmagnetic ($\mu = 1$) dielectric materials at both sides of the interface, at $z = 0$ we have the continuity of all three components of the magnetic field $\mathbf{B}_{\mathbf{q}}$, and the continuity of E_x , E_y , and $D_z \equiv \epsilon_z E_z$. However, as follows from (9), the continuity of both tangential components of the electric field immediately implies the continuity of B_z . Furthermore, since

$$\epsilon_z E_z \propto [\text{curl} \mathbf{B}]_z \propto q_x B_y - q_y B_x, \quad (50)$$

the continuity of $D_z = \epsilon_z E_z$ is a direct consequence of the continuity of the tangential magnetic field. Therefore, out of six boundary conditions here only four are actually independent, consistent with the four independent amplitudes a_s , a_p , a_+ , and a_- .

Imposing the continuity of E_x , E_y , $\epsilon_z E_z$, and $\partial_z B_z \propto (q_x B_y + q_y B_x)$, we obtain

$$\mathcal{N} \begin{pmatrix} a_s \\ a_p \\ a_+ \\ a_- \end{pmatrix} = 0, \quad (51)$$

where the matrix \mathcal{N} is defined as

$$\mathcal{N} = \begin{pmatrix} \frac{i q_y}{q_x} & i & \kappa_+ (q_y^2 - \Delta_y^+) & \kappa_- (q_y^2 - \Delta_y^-) \\ -\frac{i q_x}{q_y} & i & \kappa_+ (q_x^2 - \Delta_x^+) & \kappa_- (q_x^2 - \Delta_x^-) \\ 0 & \frac{i q^2 \epsilon_0}{\kappa_0 \epsilon_z} & \Delta_x^+ \Delta_y^+ - q_x^2 q_y^2 & \Delta_x^- \Delta_y^- - q_x^2 q_y^2 \\ \frac{i q^2 \kappa_0}{q_x q_y} & 0 & (\epsilon_y - \epsilon_x) \frac{\omega^2 \kappa_{\pm}^2}{c^2} & (\epsilon_y - \epsilon_x) \frac{\omega^2 \kappa_{\pm}^2}{c^2} \end{pmatrix}, \quad (52)$$

with

$$\Delta_{x,y}^{\pm} \equiv \Delta_{x,y}(\kappa_{\pm}). \quad (53)$$

Introducing the new variable ζ_{\pm} corresponding to the z components of the amplitudes of the electric field in the anisotropic material (\mathbf{e}_+) $_z$ and (\mathbf{e}_-) $_z$,

$$\zeta_{\pm} = (\Delta_x^{\pm} \Delta_y^{\pm} - q_x^2 q_y^2) a_{\pm}, \quad (54)$$

from (51) and (52) we obtain

$$\mathcal{P}(\omega; \mathbf{q}) \begin{pmatrix} \zeta_+ \\ \zeta_- \end{pmatrix} = 0, \quad (55)$$

where the matrix \mathcal{P} is defined by

$$\mathcal{P}(\omega; \mathbf{q}) = \begin{pmatrix} \alpha_+ & \alpha_- \\ \beta_+ & \beta_- \end{pmatrix} \quad (56)$$

and

$$\alpha_{\pm} = \frac{\epsilon_z}{\epsilon_0} + \frac{\kappa_{\pm}}{\kappa_0} \frac{(\frac{\omega}{c})^2 (\epsilon_x q_y^2 + \epsilon_y q_x^2) - q^2 (q^2 - \kappa_{\pm}^2)}{\Delta_x^{\pm} \Delta_y^{\pm} - q_x^2 q_y^2}, \quad (57)$$

$$\beta_{\pm} = \kappa_{\pm} \frac{\kappa_0 + \kappa_{\pm}}{\Delta_x^{\pm} \Delta_y^{\pm} - q_x^2 q_y^2}. \quad (58)$$

The dispersion of the surface wave is then given by

$$\det[\mathcal{P}(\omega; \mathbf{q})] = 0, \quad (59)$$

which yields

$$\begin{aligned} & \kappa_0 (\kappa_+ + \kappa_-) \left\{ \frac{\epsilon_x \epsilon_y}{\epsilon_0} \left(\left(\frac{\omega}{c} \right)^2 - \frac{q_x^2}{\epsilon_y} - \frac{q_y^2}{\epsilon_x} \right) - \kappa_+ \kappa_- \right\} \\ & + \kappa_+ \kappa_- \left\{ (\epsilon_x + \epsilon_y) \left(\frac{\omega}{c} \right)^2 - \frac{\epsilon_0 + \epsilon_x}{\epsilon_0} q_x^2 - \frac{\epsilon_0 + \epsilon_y}{\epsilon_0} q_y^2 \right\} \\ & + \left\{ \frac{\epsilon_x \epsilon_y}{\epsilon_0} \kappa_0^2 \left(\left(\frac{\omega}{c} \right)^2 - \frac{q_x^2}{\epsilon_y} - \frac{q_y^2}{\epsilon_x} \right) - \kappa_+^2 \kappa_-^2 \right\} = 0. \end{aligned} \quad (60)$$

Equation (42) uniquely defines the dispersion relation of the Dyakonov surface wave $\omega(\mathbf{q})$ and is the primary result of this section.

For a guided surface wave, all its components, in both the isotropic and anisotropic sides of the interface, must decay away from the boundary. For $z < 0$, this implies that

$$q > \sqrt{\epsilon_0} \frac{\omega}{c}. \quad (61)$$

At the same time, in the anisotropic medium the waves with the in-plane momentum \mathbf{q} can belong to either the evanescent

or ghost subclasses—see Sec. II. From Eqs. (22) and (23) we therefore obtain

$$q > \sqrt{\epsilon_z} \frac{\omega}{c} \quad (62)$$

and

$$\frac{q_x^2}{\epsilon_y} + \frac{q_y^2}{\epsilon_x} > \left(\frac{\omega}{c}\right)^2. \quad (63)$$

Equations (61), (62), and (63) substantially reduce the range of the momentum and frequency that needs to be explored in the numerical solution of Eq. (60). Furthermore, as shown in Ref. [21] (see also Appendix A), the Dyakonov surface wave only exists when

$$\min(\epsilon_x, \epsilon_y) \leq \epsilon_z < \epsilon_0 < \max(\epsilon_x, \epsilon_y). \quad (64)$$

While the numerical solution of Eq. (42) is generally straightforward, for small-to-moderate anisotropy, the surface waves are known [21,22] to be relatively weakly guided,

$$\kappa_0 \ll \omega/c, \quad (65)$$

which turns numerical root finding into a challenging numerical problem [21]. In the next section we will therefore develop the method for the analytical solution of Eq. (60).

V. ANALYTICAL SOLUTION FOR THE SURFACE WAVE DISPERSION

Despite its relative complexity, Eq. (60) is not transcendental, but only contains algebraic functions. As a result, it can be reduced to a polynomial equation. Furthermore, as we show in the present section, the resulting polynomial equation is of the fourth order, and therefore allows a complete analytical solution.

Choosing the y direction at the one corresponding to the largest permittivity in the plane of the interface,

$$\epsilon_y > \epsilon_x, \quad (66)$$

we introduce the new variable

$$u = \frac{\epsilon_x \epsilon_y}{\epsilon_0} \left(\frac{q_x^2}{\epsilon_y} + \frac{q_y^2}{\epsilon_x} - \left(\frac{\omega}{c}\right)^2 \right). \quad (67)$$

Note that, as follows from (63), $u > 0$. Then

$$\kappa_+^2 \kappa_-^2 = \frac{\epsilon_0}{\epsilon_z} \left(q^2 - \epsilon_z \left(\frac{\omega}{c}\right)^2 \right) u \quad (68)$$

and

$$\begin{aligned} \kappa_+ + \kappa_- = & \left[q^2 + \frac{\epsilon_0}{\epsilon_z} u - \left(\epsilon_x + \epsilon_y - \frac{\epsilon_x \epsilon_y}{\epsilon_z} \right) \left(\frac{\omega}{c}\right)^2 \right. \\ & \left. + 2 \sqrt{\frac{\epsilon_0}{\epsilon_z} \left(\epsilon_z \left(\frac{\omega}{c}\right)^2 - q^2 \right) u} \right]^{1/2}. \end{aligned} \quad (69)$$

We can then express Eq. (60) as

$$\kappa_0(\kappa_+ + \kappa_-)(u + \kappa_+ \kappa_-) = \hat{A} \kappa_+ \kappa_- + \hat{B}, \quad (70)$$

where

$$\hat{A} = \left(\epsilon_x + \epsilon_y - \frac{\epsilon_x \epsilon_y}{\epsilon_z} \right) \left(\frac{\omega}{c}\right)^2 - q^2 - \frac{\epsilon_0}{\epsilon_z} u \quad (71)$$

and

$$\hat{B} = -\kappa_0^2 u - \kappa_+^2 \kappa_-^2. \quad (72)$$

We then square both sides of Eq. (70), which yields

$$\hat{G} \kappa_+ \kappa_- = \hat{F}, \quad (73)$$

where

$$\begin{aligned} \hat{G} = & \epsilon_0 \left\{ \left(\frac{\epsilon_x \epsilon_y}{\epsilon_0} - \epsilon_x - \epsilon_y + \epsilon_0 \right) \left(\frac{\omega}{c}\right)^2 \right. \\ & + \left[\left(\frac{\epsilon_x}{\epsilon_0} + \frac{\epsilon_y - \epsilon_0}{\epsilon_z} - \frac{\epsilon_x \epsilon_y}{\epsilon_0^2} \right) q_x^2 \right. \\ & \left. \left. + \left(\frac{\epsilon_y}{\epsilon_0} + \frac{\epsilon_x - \epsilon_0}{\epsilon_z} - \frac{\epsilon_x \epsilon_y}{\epsilon_0^2} \right) q_y^2 \right] \right\}, \quad (74) \\ = & 2\epsilon_0 \left\{ \left(1 - \frac{\epsilon_0}{\epsilon_z} \right) u + \kappa_0^2 \left(\frac{\epsilon_x + \epsilon_y - \epsilon_0}{\epsilon_z} - \frac{\epsilon_x \epsilon_y}{\epsilon_0^2} \right) \right. \\ & \left. + \left(\frac{1}{\epsilon_0} - \frac{1}{\epsilon_z} \right) [\epsilon_0^2 - \epsilon_0(\epsilon_x + \epsilon_y) + \epsilon_x \epsilon_y] \left(\frac{\omega}{c}\right)^2 \right\}, \quad (75) \end{aligned}$$

and

$$\begin{aligned} \hat{F} = & -\epsilon_0 \left(1 - \frac{\epsilon_0}{\epsilon_z} \right) \left\{ \left(\epsilon_2 \left(\frac{\omega}{c}\right)^2 - u \right)^2 \right. \\ & \left. - \epsilon_0 \left(1 - \frac{\epsilon_0}{\epsilon_z} \right) \left(\frac{\omega}{c}\right)^2 u \right\} \\ & + \kappa_0^2 \left\{ \epsilon_0 \left[\frac{\epsilon_z^2}{\epsilon_z} + \left(1 - \frac{\epsilon_0}{\epsilon_z} \right) (\epsilon_1 + 2\epsilon_2) \right] \left(\frac{\omega}{c}\right)^2 \right. \\ & \left. - \left(\epsilon_1 + \frac{\epsilon_0}{\epsilon_z} (\epsilon_0 + 2\epsilon_2) - \frac{\epsilon_0^3}{\epsilon_z^2} \right) u \right\} \\ & - \kappa_0^4 \left\{ \frac{\epsilon_0}{\epsilon_z} (\epsilon_1 + 2\epsilon_2) \right\}, \quad (76) \end{aligned}$$

with

$$\epsilon_1 = \epsilon_0 - \epsilon_x - \epsilon_y + \frac{\epsilon_x \epsilon_y}{\epsilon_z} \quad (77)$$

and

$$\epsilon_2 = \epsilon_x + \epsilon_y - \epsilon_0 - \frac{\epsilon_x \epsilon_y}{\epsilon_0} = \frac{(\epsilon_0 - \epsilon_x)(\epsilon_y - \epsilon_0)}{\epsilon_0}. \quad (78)$$

Note that, in addition to the solutions of the original equation (60), the new Eq. (73) contains spurious roots corresponding to $\hat{A} \kappa_+ \kappa_- + \hat{B} < 0$. We therefore need to constrain the solutions of (73) with the inequality

$$\hat{A} \kappa_+ \kappa_- + \hat{B} > 0. \quad (79)$$

Together, Eqs. (73) and (79) are equivalent to the original equation (60).

Since $u > 0$ and $q > \sqrt{\epsilon_z} \omega/c$ [see Eqs. (22), (23), and (67)], from Eq. (68) we find

$$\kappa_+ \kappa_- = \kappa_z \sqrt{\frac{\epsilon_0}{\epsilon_z}} u, \quad (80)$$

where

$$\kappa_z = \sqrt{q^2 - \epsilon_z(\omega/c)^2}. \quad (81)$$

Substituting (80) into (73), we obtain

$$\kappa_z \hat{G} \sqrt{\frac{\epsilon_0}{\epsilon_z}} u = \hat{F}. \quad (82)$$

Introducing the new dimensionless variable

$$\chi \equiv \frac{c}{\omega} \kappa_z, \quad (83)$$

we can express Eq. (82) in the form

$$a_4 \chi^4 + a_3 \chi^3 + a_2 \chi^2 + a_1 \chi + a_0 = 0, \quad (84)$$

where

$$a_4 = \frac{\epsilon_0}{\epsilon_z} (\epsilon_1 + 2\epsilon_2), \quad (85)$$

$$a_3 = \sqrt{\frac{\epsilon_x \epsilon_y}{\epsilon_z}} \hat{u} 2\epsilon_0 \left(\frac{\epsilon_x + \epsilon_y - \epsilon_0}{\epsilon_z} - \frac{\epsilon_x \epsilon_y}{\epsilon_0^2} \right), \quad (86)$$

$$a_2 = -\frac{\epsilon_0 \epsilon_2^2}{\epsilon_z} + \epsilon_0 (\epsilon_1 + 2\epsilon_2) \left(1 - \frac{\epsilon_0}{\epsilon_z} \right) + \hat{u} \frac{\epsilon_x \epsilon_y}{\epsilon_0} \left[\epsilon_1 + 2\frac{\epsilon_0 \epsilon_2}{\epsilon_z} + \frac{\epsilon_0^2}{\epsilon_z} \left(1 - \frac{\epsilon_0}{\epsilon_z} \right) \right], \quad (87)$$

$$a_1 = 2 \left(1 - \frac{\epsilon_0}{\epsilon_z} \right) \sqrt{\frac{\epsilon_x^3 \epsilon_y^3}{\epsilon_z}} \hat{u} \left(1 - \frac{\epsilon_z}{\epsilon_0} + \hat{u} \right), \quad (88)$$

$$a_0 = \left(1 - \frac{\epsilon_0}{\epsilon_z} \right) \frac{\epsilon_x \epsilon_y}{\epsilon_0} \hat{u} (\epsilon_1 \epsilon_z + \epsilon_x \epsilon_y \hat{u}), \quad (89)$$

and

$$\hat{u} \equiv \frac{\epsilon_0}{\epsilon_x \epsilon_y} \left(\frac{c}{\omega} \right)^2 u = \left(\frac{c}{\omega} \right)^2 \left(\frac{q_x^2}{\epsilon_y} + \frac{q_y^2}{\epsilon_x} \right) - 1. \quad (90)$$

The expression (84) is a quartic equation for χ , and allows an immediate analytical solution via the Ferrari formula [27], so that

$$\chi = \mathcal{F}(\hat{u}; \epsilon_0, \epsilon_x, \epsilon_y, \epsilon_z). \quad (91)$$

Then, introducing the polar angle θ that defines the direction of the in-plane momentum \mathbf{q} ,

$$q_x = q \cos \theta, \quad (92)$$

$$q_y = q \sin \theta, \quad (93)$$

from (67) and (91) we obtain

$$\frac{\omega}{c} = \frac{q}{\sqrt{\epsilon_z + \mathcal{F}^2(\hat{u})}}, \quad (94)$$

$$\sin \theta = \pm \sqrt{\frac{\epsilon_x \epsilon_y}{|\epsilon_y - \epsilon_x|} \left(\frac{\hat{u} + 1}{\epsilon_z + \mathcal{F}^2(\hat{u})} - \frac{1}{\epsilon_y} \right)}, \quad (95)$$

which parametrically defines the function $\omega(q, \theta)$.

In general, a quartic equation like (84) has four distinct roots. However, in our case χ should satisfy a number of additional constraints. Aside from being a positive real quantity, it must also exceed the value of $\sqrt{\epsilon_0 - \epsilon_z}$,

$$\chi > \sqrt{\epsilon_0 - \epsilon_z}, \quad (96)$$

since decay of the surface wave away from the interface implies

$$\kappa_0 = \frac{\omega}{c} \sqrt{\chi^2 + \epsilon_z - \epsilon_0} > 0. \quad (97)$$

As we prove in Appendix B, Eq. (84) only has no more than a single real positive solution that satisfies (96), so there is no ambiguity in choosing the correct root. We therefore obtain

$$\mathcal{F} = -\frac{a_3}{4a_4} + s_1 S + \frac{s_2}{2} \sqrt{-4S^2 - 2\hat{p} - \frac{s_1 \cdot \hat{q}}{S}}, \quad (98)$$

where

$$\hat{p} = \frac{a_2}{a_4} - \frac{3}{8} \frac{a_3^2}{a_4^2}, \quad (99)$$

$$\hat{q} = \frac{a_3^3 - 4a_2 a_3 a_4 + 8a_1 a_4^2}{8a_4^3}, \quad (100)$$

$$S = \frac{1}{2} \sqrt{-\frac{2}{3} \hat{p} + \frac{1}{3a_4} \left(Q + \frac{\Delta_0}{Q} \right)}, \quad (101)$$

$$Q = \sqrt[3]{\frac{\Delta_1 + \sqrt{\Delta_1^2 - 4\Delta_0^3}}{2}}, \quad (102)$$

$$\Delta_0 = a_2^2 - 3a_1 a_2 + 12a_0 a_4, \quad (103)$$

$$\Delta_1 = 2a_2^3 - 9a_1 a_2 a_3 + 27a_0 a_3^2 + 27a_1^2 a_4 - 72a_0 a_2 a_4, \quad (104)$$

$$s_{1,2} = \pm 1. \quad (105)$$

While the choice of s_1 and s_2 in Eq. (105) that leads to a positive real root that satisfies Eq. (96) is unique, such a solution only exists in a limited range of angles θ . Furthermore, the resulting solution must be tested against the inequality (79) to remove the spurious roots. As a result, for the angular range of θ that supports the Dyakonov surface wave, we obtain (see Appendix C)

$$\theta_1 < |\theta| < \theta_2 \quad \text{or} \quad \pi - \theta_2 < |\theta| < \pi - \theta_1, \quad (106)$$

where, assuming $\epsilon_y > \epsilon_x$,

$$\theta_1 = \arcsin \left\{ \left[\frac{\epsilon_x \epsilon_y}{\epsilon_y - \epsilon_x} \left(\frac{\epsilon_1 + 2\epsilon_2}{(\epsilon_1 + 2\epsilon_2) + \epsilon_2^2} - \frac{1}{\epsilon_y} \right) \right]^{1/2} \right\} \quad (107)$$

and

$$\theta_2 = \arcsin \left\{ \left[\left(1 - \sqrt{1 + \frac{4\epsilon_z(\epsilon_0 - \epsilon_x)(\epsilon_y - \epsilon_0)}{\epsilon_0^2(\epsilon_0 - \epsilon_z)}} \right) \times \frac{\epsilon_0}{2\epsilon_z} \frac{\epsilon_0 - \epsilon_z}{\epsilon_y - \epsilon_x} + \frac{\epsilon_y - \epsilon_0}{\epsilon_y - \epsilon_x} \right]^{1/2} \right\}. \quad (108)$$

Here, θ_1 and θ_2 correspond to $\kappa_- = 0$ and $\kappa_0 = 0$, respectively. At the same time, θ_1 corresponds to the boundary of the inequality (63), while θ_2 represents the ‘‘edge’’ of the inequality (79)—see Appendix C. Within the angle range (106) for any direction θ and the frequency ω , there is one and only one surface wave, described by the parametric equations (94) and

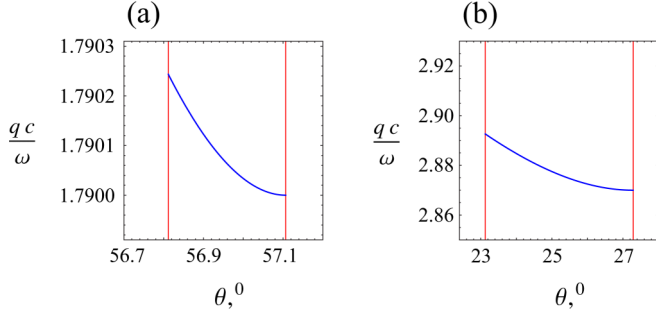


FIG. 6. In-plane wave number of the Dyakonov surface wave (in units of ω/c) vs the propagation direction angle θ in biaxial materials, for the interfaces of (a) potassium titanyl phosphate (KTP) with aluminium oxynitride (AlON) and (b) arsenic trisulfide with aluminum arsenide. The corresponding refractive indices are [28] as follows. KTP: $n_x = 1.7614$, $n_y = 1.8636$, $n_z = 1.7704$; AlON: $n_0 = 1.79$; arsenic trisulfide: $n_x = 2.4$, $n_y = 3.02$, $n_z = 2.81$; aluminum arsenide: $n_0 = 2.87$.

(95) with the function $\mathcal{F}(\hat{u}, \epsilon_0, \epsilon_x, \epsilon_y, \epsilon_z)$ from Eq. (98), while for any angle outside this range, there is no surface wave.

In Fig. 6 we plot the surface wave dispersion for the interface of potassium titanyl phosphate (KTP) and aluminium oxynitride (AlON) (a) and arsenic trisulfide with aluminum arsenide (b). The results of the present work can also be applied to uniaxial materials, as illustrated in Fig. 7 for calcite and CdF_2 (a) and lithium niobate (LiNbO_3) and KTaO_3 (b).

Following Ref. [21], it is also instructive to project the surface wave dispersion onto the wave-vector space (q_x, q_y) that we studied in Sec. II. In Fig. 8 we show this projection for the surface wave at the interface of isotropic aluminum arsenide and biaxial arsenic trisulfide. As expected, the magenta curve that represents the Dyakonov surface wave terminates at the boundaries corresponding to $\kappa_0 = 0$ (blue line) and $\kappa_- = 0$ (green line). Note that, depending on the wave vector of the surface wave, it could be observed both in the “evanescent” and “ghost” portions of the phase space [see panel (c)].

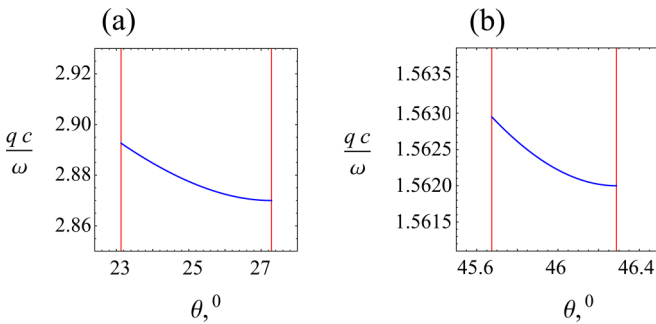


FIG. 7. In-plane wave number of the Dyakonov surface wave (in units of ω/c) vs the propagation direction angle θ in uniaxial materials, for the interfaces of (a) calcite with CdF_2 and (b) lithium niobate and KTaO_3 . The corresponding refractive indices are [28] as follows. Calcite: $n_x = n_z = 1.486$, $n_y = 1.658$; CdF_2 : $n_0 = 1.562$; lithium niobate: $n_x = n_z = 2.156$, $n_y = 2.232$; KTaO_3 : $n_0 = 2.2$.

VI. TWO CLASSES OF DYAKONOV SURFACE WAVES

Near the boundary of an isotropic medium with a uniaxial dielectric, the Dyakonov surface wave is formed by evanescent waves on both sides of the interface. However, for a biaxial dielectric that supports both the evanescent and the ghost waves (see Sec. II), the localized surface wave can be formed from either the evanescent or from ghost waves, depending on its in-plane momentum. As a result, for the interface of an isotropic medium with a biaxial medium, we can have two different types of the Dyakonov surface wave. A “conventional” Dyakonov surface wave, as originally described by Dyakonov in 1988 [18], monotonically decays on both sides of the interface, while the ghost surface wave together with the exponential decay also shows oscillatory behavior in the anisotropic medium—see Fig. 9.

Note that, depending on the magnitude of the permittivity of the isotropic medium ϵ_0 ($\epsilon_z < \epsilon_0 < \epsilon_y$), at a single frequency the isotropic–biaxial interface can either support both the conventional and the ghosts mode patterns, or only the conventional modes. The corresponding critical value ϵ_c of the permittivity ϵ_0 is given by the equation (see Appendix D)

$$\begin{aligned} & (\epsilon_c - \epsilon_z)^2 \left(5\epsilon_z - 3(\epsilon_x + \epsilon_y) + \frac{\epsilon_x \epsilon_y}{\epsilon_z} \right) \\ & + (\epsilon_c - \epsilon_z) \left[\epsilon_x^2 + 4\epsilon_x \epsilon_y + \epsilon_y^2 - 8\epsilon_z(\epsilon_x + \epsilon_y) + 10\epsilon_z^2 \right] \\ & + 3\epsilon_z(\epsilon_y - \epsilon_z)(\epsilon_z - \epsilon_x) \\ & + \frac{2}{\epsilon_z} ((\epsilon_c - \epsilon_z)^2 + \epsilon_z [2(\epsilon_x + \epsilon_y) - 5\epsilon_z]) \\ & \times \sqrt{\epsilon_z(\epsilon_y - \epsilon_z)(\epsilon_z - \epsilon_x)(\epsilon_c - \epsilon_z)} = 0, \end{aligned} \quad (109)$$

which for $\epsilon_x < \epsilon_z < \epsilon_y$ always has a single solution in the interval $\epsilon_z < \epsilon_c < \epsilon_y$.

In scaled variables ϵ_c/ϵ_z , ϵ_z/ϵ_x , and ϵ_y/ϵ_z , the solution of Eq. (109) can be expressed as

$$\frac{\epsilon_c}{\epsilon_z} = \mathcal{G} \left(\frac{\epsilon_z}{\epsilon_x}, \frac{\epsilon_y}{\epsilon_z} \right). \quad (110)$$

We plot this function in Fig. 10.

For $\epsilon_c < \epsilon_0 < \epsilon_y$, the Dyakonov surface waves that are supported by the interface of isotropic and biaxial dielectric media belong to the conventional class for all allowed propagation angles. However, if $\epsilon_z < \epsilon_0 < \epsilon_c$, for the propagation angle θ in the range $\theta_1 < |\theta| < \theta_3$ and $\pi - \theta_3 < |\theta| < \pi - \theta_1$ we find conventional Dyakonov waves, while for $\theta_3 < |\theta| < \theta_2$ and $\pi - \theta_2 < |\theta| < \pi - \theta_3$ the surface modes belong to the ghost class—see Fig. 8(c). Here, the angle θ_3 only depends on the dielectric permittivities of the media forming the interface, and is defined as the solution of the system of equations (60) and (25), where the latter are taken with the positive signs.

VII. DISCUSSION

The key feature of the Dyakonov surface waves that makes them an ideal platform for experiments on nonlinear optics and strong coupling is their inherent “lossless” nature. While the residual linear absorption in the dielectric as well as light scattering due to surface roughness can never be completely avoided, the corresponding contributions to the effective mode

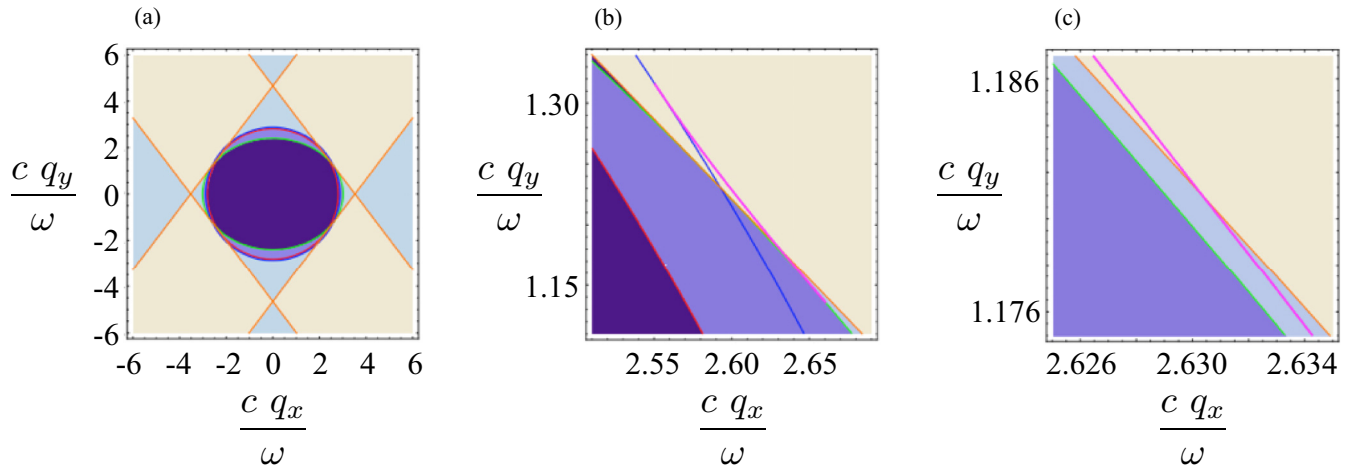


FIG. 8. Dyakonov surface wave in (q_x, q_y) coordinates for the aluminum arsenide–arsenic trisulfide interface. The surface wave is shown by the magenta line (dark gray line at higher values of q_y). The red (gray) line corresponds to Eq. (22), the green (light-gray) line represents Eq. (23), the blue line (dark gray line at lower values of q_y) corresponds to Eq. (61), and the orange (straight) lines show the ghost region boundaries from Eq. (25). The phase-space color code is the same as in Figs. 1–4. Panels (b) and (c) show the magnified portions of the phase space that supports the Dyakonov surface wave. Note that, as clearly seen in panel (c), the surface wave is supported by both the evanescent and the ghost regions of the phase space.

loss can be dramatically reduced, as demonstrated in Mie resonance experiments with the measured Q factors on the order of 10^{10} [29].

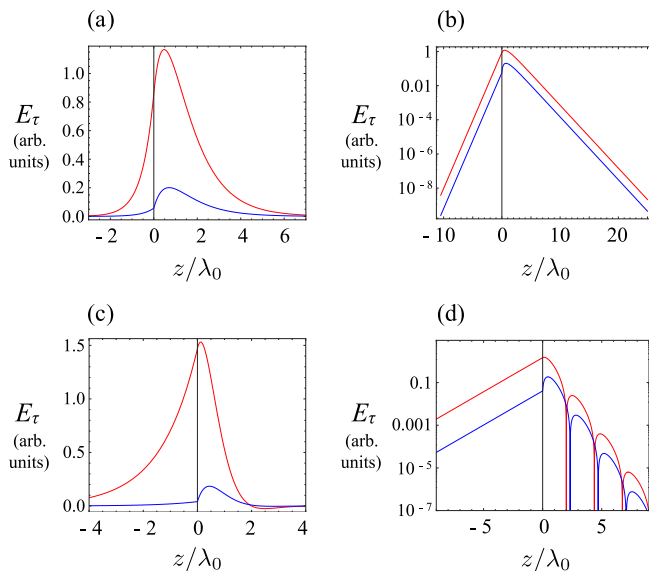


FIG. 9. Dyakonov surface waves at the arsenic trisulfide ($n_x = 2.4$, $n_y = 3.02$, $n_z = 2.81$)–aluminum arsenide ($n_0 = 2.87$) interface: “conventional” (a),(b) vs “ghost” (c),(d), in linear (a),(c) and logarithmic (b),(d) scale. Red (light gray) and blue (dark gray) curves correspond to the projections of the in-plane electric field $\mathbf{E}_\tau = (E_x, E_y)$ onto the parallel (blue, dark gray) and perpendicular (red, light gray) to the in-plane momentum \mathbf{q} directions. The in-plane propagation angle θ is equal to 24° (a),(b) and 26° (c),(d). The biaxial arsenic trisulfide is on the right of the interface $z = 0$, and the isotropic aluminum arsenide fills the half-space $z < 0$. Note the contrast of the simple exponential decay of the conventional Dyakonov waves in the biaxial medium [see panel (b)] with the oscillatory behavior of the ghost surface waves (d).

As a result, with an evanescent coupling (from, e.g., a high-index prism) to the isotropic-biaxial interface, one can observe an enormous increase of the field intensity at this boundary, only limited by the effective loss due to system imperfections (surface and bulk disorder, etc.) and ultimately by the nonlocality of the dielectric response [30] [corresponding to the variations of the dielectric permittivity on the order of $(a_0/\lambda)^2 \sim 10^{-6}$, where a_0 is on the order of the atomic size and λ is the wavelength].

For the applications to nonlinear optics, however, the effective “selection rules” such as the phase-matching conditions [31,32] are defined by the spatial variation of the

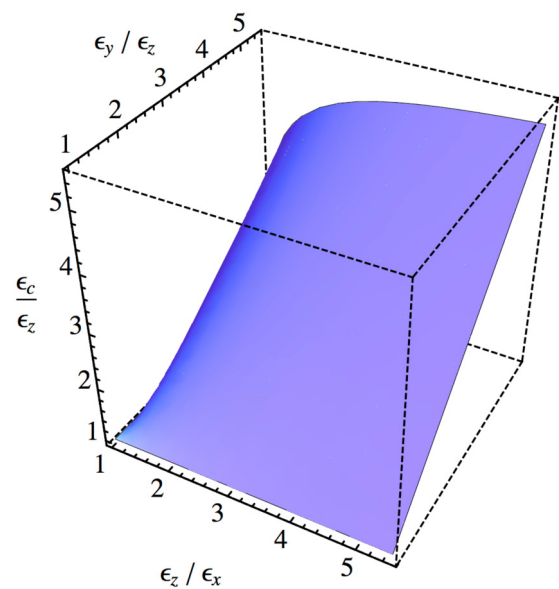


FIG. 10. Critical value ϵ_c of the isotropic medium, in units of ϵ_z vs ϵ_z/ϵ_x , ϵ_y/ϵ_z . The dielectric permittivity components of the biaxial medium satisfy $\epsilon_x < \epsilon_z < \epsilon_y$.

corresponding optical modes. The qualitative difference between the ghost and the conventional surface waves, respectively with and without oscillations away from the interface, that can be simultaneously supported by the same isotropic-biaxial interface at the same frequency, will therefore have dramatic effect on the nonlinear-optical phenomena in this system [25].

VIII. CONCLUSIONS

In summary, we have developed a complete analytical theory of Dyakonov surface waves at the interface of an isotropic medium with a biaxial anisotropic dielectric. As opposed to earlier work on this subject, our approach does not require any numerical root finding and offers substantial advantage in the description of the surface waves near the propagation threshold. We have also presented a detailed description of the ghost waves that combine the properties of propagating and evanescent solutions and of the corresponding surface modes supported by these ghost waves.

ACKNOWLEDGMENTS

This work was partially supported by the Army Research Office (Grant No. W911NF-14-1-0639), National Science Foundation (Grants No. DMR-1120923 and No. DMR-1629276), and Gordon and Betty Moore Foundation.

APPENDIX A

Some of the necessary conditions for the existence of the Dyakonov wave in (64) can be immediately obtained from the general structure of Eq. (60) and its constituents. Equation (63) immediately implies that both the first and the last terms in the curly brackets in Eq. (60) are negative definite; therefore,

$$\frac{\epsilon_0 + \epsilon_x}{\epsilon_0} q_x^2 + \frac{\epsilon_0 + \epsilon_y}{\epsilon_0} q_y^2 < (\epsilon_x + \epsilon_y) \left(\frac{\omega}{c} \right)^2. \quad (\text{A1})$$

Since

$$\begin{aligned} \frac{\epsilon_x}{\epsilon_0} q_x^2 + \frac{\epsilon_y}{\epsilon_0} q_y^2 &= \frac{\epsilon_x \epsilon_y}{\epsilon_0} \left(\frac{q_x^2}{\epsilon_y} + \frac{q_y^2}{\epsilon_x} - \left(\frac{\omega}{c} \right)^2 \right) \\ &+ \frac{\epsilon_x \epsilon_y}{\epsilon_0} \left(\frac{\omega}{c} \right)^2 > \frac{\epsilon_x \epsilon_y}{\epsilon_0} \left(\frac{\omega}{c} \right)^2, \end{aligned} \quad (\text{A2})$$

from (61) and (A1) we obtain

$$\epsilon_x + \epsilon_y > \epsilon_0 + \frac{\epsilon_x \epsilon_y}{\epsilon_0}, \quad (\text{A3})$$

which implies that

$$\min(\epsilon_x, \epsilon_y) < \epsilon_0 < \max(\epsilon_x, \epsilon_y). \quad (\text{A4})$$

Similarly, from (62), (A1), and (A2)

$$\epsilon_x + \epsilon_y > \epsilon_z + \frac{\epsilon_x \epsilon_y}{\epsilon_0} \quad (\text{A5})$$

or

$$\begin{aligned} \epsilon_z &< \max(\epsilon_x, \epsilon_y) - \min(\epsilon_x, \epsilon_y) \left(1 - \frac{\max(\epsilon_x, \epsilon_y)}{\epsilon_0} \right) \\ &< \max(\epsilon_x, \epsilon_y). \end{aligned} \quad (\text{A6})$$

APPENDIX B

First, we consider the number of real positive solutions of Eq. (84). Since

$$\epsilon_1 + 2\epsilon_2 = \frac{(\epsilon_0 - \epsilon_x)(\epsilon_y - \epsilon_0)}{\epsilon_0} + \epsilon_x \epsilon_y \left(\frac{1}{\epsilon_z} - \frac{1}{\epsilon_0} \right) > 0, \quad (\text{B1})$$

with our choice of $\epsilon_x < \epsilon_y$ [see (66)] the requirement (64) reduces to

$$\epsilon_x \leq \epsilon_z < \epsilon_0 < \epsilon_y, \quad (\text{B2})$$

and therefore

$$a_4 > 0. \quad (\text{B3})$$

Similarly, since $\hat{u} > 0$,

$$a_1 < 0 \quad (\text{B4})$$

and

$$\begin{aligned} a_3 &= \sqrt{\frac{\epsilon_x \epsilon_y}{\epsilon_0}} \hat{u} 2\epsilon_0 \left(\frac{\epsilon_x + \epsilon_y - \epsilon_0}{\epsilon_z} - \frac{\epsilon_x \epsilon_y}{\epsilon_0^2} \right) \\ &= \frac{2}{\epsilon_z} \sqrt{\frac{\epsilon_x \epsilon_y}{\epsilon_0}} \hat{u} \left((\epsilon_0 - \epsilon_x)(\epsilon_y - \epsilon_0) + \frac{\epsilon_x \epsilon_y}{\epsilon_0} (\epsilon_0 - \epsilon_z) \right) \\ &> 0. \end{aligned} \quad (\text{B5})$$

Therefore, regardless of the sign of a_2 , the number of sign changes of the polynomial $a_4 \chi^4 + a_3 \chi^3 + a_2 \chi^2 + a_1 \chi + a_0$ is equal to one if $a_0 < 0$ and to two if $a_0 > 0$. According to Descartes' rule of signs [33], Eq. (84) has no more than one positive real root in the former case and no more than two positive real roots in the latter. So, in general, Eq. (84) has no more than two positive real roots.

However, the solution of Eq. (84) must also satisfy the inequality (96). Introducing the new variable

$$\xi \equiv \chi - \sqrt{\epsilon_0 - \epsilon_z}, \quad (\text{B6})$$

to satisfy (96) we need $\xi > 0$. From (84) we obtain

$$a_4 \xi^4 + b_3 \xi^3 + b_2 \xi^2 + b_1 \xi + b_0 = 0, \quad (\text{B7})$$

where

$$b_3 = a_3 + 4a_4 \sqrt{\epsilon_0 - \epsilon_z}, \quad (\text{B8})$$

$$b_2 = a_2 + 3a_3 \sqrt{\epsilon_0 - \epsilon_z} + 6a_4 (\epsilon_0 - \epsilon_z), \quad (\text{B9})$$

$$b_1 = a_1 + 2a_2 \sqrt{\epsilon_0 - \epsilon_z} + 3a_3 (\epsilon_0 - \epsilon_z) + 4a_4 (\epsilon_0 - \epsilon_z)^{3/2}, \quad (\text{B10})$$

$$\begin{aligned} b_0 &= a_0 + a_1 \sqrt{\epsilon_0 - \epsilon_z} + a_2 (\epsilon_0 - \epsilon_z) \\ &+ a_3 (\epsilon_0 - \epsilon_z)^{3/2} + a_4 (\epsilon_0 - \epsilon_z)^2. \end{aligned} \quad (\text{B11})$$

From (B3) and (B5)

$$b_3 > 0. \quad (\text{B12})$$

For b_0 we obtain

$$\begin{aligned} b_0 &= -\frac{\epsilon_0 - \epsilon_z}{\epsilon_0 \epsilon_z} \left(\epsilon_x \epsilon_y \hat{u} + \epsilon_0 \sqrt{\frac{\epsilon_x \epsilon_y}{\epsilon_z}} (\epsilon_0 - \epsilon_z) \hat{u} \right. \\ &\left. - (\epsilon_0 - \epsilon_x)(\epsilon_y - \epsilon_0) \right)^2 < 0. \end{aligned} \quad (\text{B13})$$

If either $b_1 > 0, b_2 > 0$ or $b_1 < 0, b_2 < 0$ or $b_1 < 0, b_2 > 0$, then the number of sign changes of the polynomial $a_4\chi^4 + a_3\chi^3 + a_2\chi^2 + a_1\chi + a_0$ is equal to one, and therefore Eq. (B7) has no more than one real positive root. It is if and only if $b_1 > 0, b_2 < 0$ that Eq. (B7) can in principle have two positive real roots.

For $b_1 > 0, b_2 < 0$, from Eqs. (B9) and (B10) we obtain

$$a_2 + 3a_3\sqrt{\epsilon_0 - \epsilon_z} + 6a_4(\epsilon_0 - \epsilon_z) < 0, \quad (\text{B14})$$

$$a_1 + 2a_2\sqrt{\epsilon_0 - \epsilon_z} + 3a_3(\epsilon_0 - \epsilon_z) + 4a_4(\epsilon_0 - \epsilon_z)^{3/2} > 0. \quad (\text{B15})$$

Then

$$a_2 < -3a_3\sqrt{\epsilon_0 - \epsilon_z} - 6a_4(\epsilon_0 - \epsilon_z) \quad (\text{B16})$$

and

$$3a_3(\epsilon_0 - \epsilon_z) + 4a_4(\epsilon_0 - \epsilon_z)^{3/2} > -a_1 - 2a_2\sqrt{\epsilon_0 - \epsilon_z} > -a_1 + 2(\epsilon_0 - \epsilon_z)(3a_3 + 6a_4\sqrt{\epsilon_0 - \epsilon_z}), \quad (\text{B17})$$

which yields

$$-3a_3 - 8a_4\sqrt{\epsilon_0 - \epsilon_z} > -\frac{a_1}{\epsilon_0 - \epsilon_z}. \quad (\text{B18})$$

With $a_1 < 0, a_3 > 0$, and $a_4 > 0$, and $\epsilon_0 > \epsilon_z$ [see (64)], the left-hand side of (B18) is negative, while the right-hand side is positive. The system of the inequalities (B14),(B15) is therefore inconsistent and the case $b_1 > 0, b_2 < 0$ cannot be realized. Therefore, Eq. (B7) cannot have more than one positive real root and Eq. (84) cannot have more than one real solution with $\chi > \sqrt{\epsilon_0 - \epsilon_z}$.

APPENDIX C

We define θ_1 as the propagation angle that corresponds to the limiting case of the inequality (63). In terms of our parameter \hat{u} defined by Eqs. (67) and (90), the bound (63) corresponds to

$$\hat{u}(\theta_1) = u(\theta_1) = 0, \quad (\text{C1})$$

which together with (68) implies that

$$\kappa_-(\theta_1) = 0. \quad (\text{C2})$$

Since

$$a_0(\hat{u} = 0) = a_1(\hat{u} = 0) = a_3(\hat{u} = 0) = 0, \quad (\text{C3})$$

we obtain

$$\begin{aligned} \mathcal{F}(\hat{u} = 0) &= \sqrt{-\frac{a_2(\hat{u} = 0)}{a_4(\hat{u} = 0)}} \\ &= \sqrt{\epsilon_0 - \epsilon_z + \frac{\epsilon_z^2}{\epsilon_1 + 2\epsilon_2}}. \end{aligned} \quad (\text{C4})$$

Substituting (C1) into (95), we obtain

$$\sin^2 \theta_1 = \frac{\epsilon_x \epsilon_y}{\epsilon_y - \epsilon_x} \left(\frac{\epsilon_a + 2\epsilon_2}{\epsilon_0(\epsilon_1 + 2\epsilon_2) + \epsilon_z^2} - \frac{1}{\epsilon_y} \right), \quad (\text{C5})$$

leading to our definition of θ_1 in Eq. (107).

Since we defined the x and y directions with $\epsilon_y > \epsilon_x$, the inequality (63) then implies

$$\theta_1 < |\theta| < \pi/2 \quad (\text{C6})$$

or

$$\pi/2 < |\theta| < \pi - \theta_1. \quad (\text{C7})$$

The angle θ_2 is defined as the propagation direction of the surface wave corresponding to the limiting case of (79) when the latter turns into the exact equality

$$\hat{A}(\theta_2)\kappa_+(\theta_2)\kappa_-(\theta_2) + \hat{B}(\theta_2) = 0. \quad (\text{C8})$$

Substituting (C8) into (70), we find that either

$$\kappa_0(\theta_2) = 0 \quad (\text{C9})$$

or

$$-\frac{\epsilon_x \epsilon_y}{\epsilon_0} \hat{u}(\theta_2) \left(\frac{\omega}{c} \right)^2 = \kappa_+(\theta_2)\kappa_-(\theta_2). \quad (\text{C10})$$

Since for θ in the range defined by Eqs. (C6) and (C7) we find $\hat{u} > 0$, and Eq. (C10) therefore cannot be satisfied—so that (C9) is the only option. Then, substituting (C9) into Eq. (60), we obtain

$$\left(\epsilon_2 - \frac{\epsilon_x \epsilon_y}{\epsilon_0} \hat{u}(\theta_2) \right) \left(\frac{\omega}{c} \right)^2 = \kappa_+(\theta_2)\kappa_-(\theta_2). \quad (\text{C11})$$

From (68) we obtain

$$\kappa_+(\theta_2)\kappa_-(\theta_2) = \left(\frac{\omega}{c} \right)^2 \sqrt{\frac{\epsilon_x \epsilon_y}{\epsilon_z} (\epsilon_0 - \epsilon_z) \hat{u}(\theta_2)}. \quad (\text{C12})$$

Substituting (C12) into (C11), we find

$$\begin{aligned} \hat{u}(\theta_2) &= \frac{\epsilon_0 \epsilon_2}{\epsilon_x \epsilon_y} + \frac{\epsilon_0^2 (\epsilon_0 - \epsilon_z)}{2\epsilon_x \epsilon_y \epsilon_z} \\ &\times \left(1 - \sqrt{1 + \frac{4\epsilon_z (\epsilon_0 - \epsilon_x) (\epsilon_y - \epsilon_0)}{\epsilon_0^2 (\epsilon_0 - \epsilon_z)}} \right). \end{aligned} \quad (\text{C13})$$

From (90) and (C9)

$$\hat{u}(\theta_2) = \frac{\epsilon_0}{\epsilon_y} \cos^2 \theta_2 + \frac{\epsilon_0}{\epsilon_x} \sin^2 \theta_2 - 1. \quad (\text{C14})$$

Substituting (C13) into (C14) and using (78), we find

$$\begin{aligned} \sin^2 \theta_2 &= \frac{\epsilon_y - \epsilon_0}{\epsilon_y - \epsilon_x} + \frac{\epsilon_0}{2\epsilon_z} \frac{\epsilon_0 - \epsilon_z}{\epsilon_y - \epsilon_x} \\ &\times \left(1 - \sqrt{1 + \frac{4\epsilon_z (\epsilon_0 - \epsilon_x) (\epsilon_y - \epsilon_0)}{\epsilon_0^2 (\epsilon_0 - \epsilon_z)}} \right). \end{aligned} \quad (\text{C15})$$

To satisfy Eq. (79), we therefore need

$$0 < |\theta| < \theta_2 \quad (\text{C16})$$

or

$$\pi - \theta_2 < |\theta| < \pi. \quad (\text{C17})$$

Together, Eqs. (C6), (C7) and (C16), (C17) are equivalent to (106).

APPENDIX D

The critical angle θ_1 corresponds to the point where the isofrequency curve of the Dyakonov surface wave in the (q_x, q_y) space terminates at the line (23). We can show that the ghost boundary in the first quadrant,

$$\sqrt{\frac{\epsilon_z - \epsilon_x}{\epsilon_z}} q_x + \sqrt{\frac{\epsilon_y - \epsilon_z}{\epsilon_z}} q_y = \sqrt{\epsilon_y - \epsilon_x} \frac{\omega}{c}, \quad (\text{D1})$$

can never cross this point. An assumption that such an intersection point $(q_x^{(1)}, q_y^{(1)})$, that satisfies both (23) and (D1), may exist leads to the equation

$$\left(q_x^{(1)} - \epsilon_y \frac{\omega}{c} \sqrt{\frac{(\epsilon_y - \epsilon_z)(\epsilon_z - \epsilon_x)}{\epsilon_z(\epsilon_y - \epsilon_x)}} \right)^2 + \left(\frac{\omega}{c} \right)^2 \frac{\epsilon_y^2 (\epsilon_z - \epsilon_x)^2}{\epsilon_z (\epsilon_y - \epsilon_x)^2} = 0, \quad (\text{D2})$$

which cannot be satisfied for any $\epsilon_x < \epsilon_z < \epsilon_y$. As a result, in the first quadrant ($q_x > 0, q_y > 0$) the ghost boundary is either always above or always below the curve of Eq. (23). The ellipse of Eq. (23) intersects the positive half of the q_y axis at the point of $\sqrt{\epsilon_x} \omega/c$, while for the ghost boundary (D1) the corresponding crossing point is at $\sqrt{\epsilon_z(\epsilon_y - \epsilon_x)/(\epsilon_z - \epsilon_x)} \omega/c > \sqrt{\epsilon_x} \omega/c$. In the first quadrant of the \mathbf{q} space the ghost boundary is therefore always above the elliptical curve of Eq. (23). As a result, this boundary, and thus the θ_1 “edge” of the isofrequency curve of the Dyakonov surface wave, is *always* in the conventional regime, with the field characterized by the exponential decay on both sides of the interface.

As a result, for the system to support the ghost surface waves, the ghost boundary (D1) must cross the isofrequency curve of the Dyakonov waves, Eq. (60). The onset of the ghost regime then corresponds to the case when the ghost boundary intersects the isofrequency curve precisely at its end at the angle θ_2 .

As follows from Eq. (C9), the critical angle θ_2 corresponds to the point where the isofrequency line of the Dyakonov surface wave in the (q_x, q_y) space terminates at the circle

$$q_x^2 + q_y^2 = \epsilon_0 \frac{\omega^2}{c^2}. \quad (\text{D3})$$

For the intersection point $(q_x^{(2)}, q_y^{(2)})$ of (D3) with the ghost boundary (D1) in the first quadrant we obtain

$$q_x^{(2)} = \frac{\omega}{c} \frac{\sqrt{\epsilon_z(\epsilon_z - \epsilon_x)} + \sqrt{(\epsilon_y - \epsilon_z)(\epsilon_0 - \epsilon_z)}}{\epsilon_y - \epsilon_x}, \quad (\text{D4})$$

$$q_y^{(2)} = \frac{\omega}{c} \frac{\sqrt{\epsilon_z(\epsilon_y - \epsilon_z)} + \sqrt{(\epsilon_z - \epsilon_x)(\epsilon_0 - \epsilon_z)}}{\epsilon_y - \epsilon_x}. \quad (\text{D5})$$

Substituting (D4) and (D5) into (60) and using (68), we obtain

$$\begin{aligned} & (\epsilon_0 - \epsilon_z)^2 \left(5\epsilon_z - 3(\epsilon_x + \epsilon_y) + \frac{\epsilon_x \epsilon_y}{\epsilon_z} \right) \\ & + (\epsilon_0 - \epsilon_z) (\epsilon_x^2 + 4\epsilon_x \epsilon_y + \epsilon_y^2 - 8\epsilon_z(\epsilon_x + \epsilon_y) + 10\epsilon_z^2) \\ & + 3\epsilon_z(\epsilon_y - \epsilon_z)(\epsilon_z - \epsilon_x) \\ & + \frac{2}{\epsilon_z} ((\epsilon_c - \epsilon_z)^2 + \epsilon_z [2(\epsilon_x + \epsilon_y) - 5\epsilon_z]) \\ & \times \sqrt{\epsilon_z(\epsilon_y - \epsilon_z)(\epsilon_z - \epsilon_x)(\epsilon_0 - \epsilon_z)} = 0, \quad (\text{D6}) \end{aligned}$$

which defines the permittivity of the dielectric media corresponding to the onset of ghost surface waves in the system phase space.

-
- [1] M. Specht, J. D. Pedarnig, W. M. Heckl, and T. W. Hänsch, Scanning Plasmon Near-Field Microscope, *Phys. Rev. Lett.* **68**, 476 (1992).
- [2] D. A. Schultz, Plasmon resonant particles for biological detection, *Curr. Opin. Biotechnol.* **14**, 13 (2003).
- [3] M. L. Juan, M. Righini, and R. Quidant, Plasmon nano-optical tweezers, *Nat. Photon.* **5**, 349 (2011).
- [4] T. W. Ebbesen, C. Genet, and S. I. Bozhevolnyi, Surface-plasmon circuitry, *Phys. Today* **61**, 44 (2008).
- [5] J. B. Pendry, Negative Refraction Makes a Perfect Lens, *Phys. Rev. Lett.* **85**, 3966 (2000).
- [6] F. D. M. Haldane, Electromagnetic surface modes at interface with negative refractive index make a “not-quite-perfect” lens, [arXiv:cond-mat/0206420](https://arxiv.org/abs/cond-mat/0206420).
- [7] S. M. Nie and S. R. Emery, Probing single molecules and single nanoparticles by surface-enhanced Raman scattering, *Science* **275**, 1102 (1997).
- [8] K. Kneipp, Y. Wang, H. Kneipp, L. T. Perelman, I. Itzkan, R. R. Dasari, and M. S. Feld, Single Molecule Detection Using Surface-Enhanced Raman Scattering (SERS), *Phys. Rev. Lett.* **78**, 1667 (1997).
- [9] T. W. Ebbesen, H. J. Lezec, H. F. Ghaemi, T. Thio, and P. A. Wolff, Extraordinary optical transmission through sub-wavelength hole arrays, *Nature (London)* **391**, 667 (1998).
- [10] Surface plasmon resurrection (editorial), *Nat. Photon.* **6**, 707 (2012).
- [11] I. Tamm, On the possible bound states of electrons on a crystal surface, *Phys. Z. Soviet Union* **1**, 733 (1932).
- [12] W. Shockley, On the surface states associated with a periodic potential, *Phys. Rev.* **56**, 317 (1939).
- [13] P. Yeh, A. Yariv, and A. Y. Cho, Optical surface waves in periodic layered media, *Appl. Phys. Lett.* **32**, 104 (1978).
- [14] E. Yablonovitch, Inhibited Spontaneous Emission in Solid-State Physics and Electronics, *Phys. Rev. Lett.* **58**, 2059 (1987).
- [15] S. John, Strong Localization of Photons in Certain Disordered Dielectric Superlattices, *Phys. Rev. Lett.* **58**, 2486 (1987).
- [16] J. D. Joannopoulos, S. G. Johnson, J. N. Winn, and R. D. Meade, *Photonic Crystals: Molding the Flow of Light* (Princeton University Press, Princeton, NJ, 2008).
- [17] F. N. Marchevskii, V. L. Strizhevskii, and S. V. Strizhevskii, Singular electromagnetic waves in bounded anisotropic media, *Sov. Phys. Solid State* **26**, 857 (1984).
- [18] M. I. Dyakonov, New type of electromagnetic wave propagating at an interface, *Sov. Phys. JETP* **67**, 714 (1988).

- [19] N. S. Averkiev and M. I. Dyakonov, Electromagnetic waves localized at the interface of transparent anisotropic media, *Opt. Spectrosc. (USSR)* **68**, 653 (1990).
- [20] L. Torner, D. Artigas, and O. Takayama, Dyakonov surface waves, *Opt. Photon. News* **20**, 25 (2009).
- [21] D. B. Walker, E. N. Glytsis, and T. K. Gaylord, Surface mode at isotropic-uniaxial and isotropic-biaxial interfaces, *J. Opt. Soc. Am. A* **15**, 248 (1998).
- [22] O. Takayama, L. C. Crasovan, D. Mihalache, and L. Torner, Dyakonov surface waves: A review, *Electromagnetics* **28**, 126 (2008).
- [23] O. Takayama, L. Crasovan, D. Artigas, and L. Torner, Observation of Dyakonov Surface Waves, *Phys. Rev. Lett.* **102**, 043903 (2009).
- [24] R. Buckley and P. Berini, Figures of merit for 2D surface plasmon waveguides and application to metal stripes, *Opt. Express* **15**, 12174 (2007).
- [25] E. Narimanov, Ghost waves in anisotropic materials: negative refractive index and evanescent field enhancement in lossless media, [arXiv:1704.06435](https://arxiv.org/abs/1704.06435) [physics.optics].
- [26] J. Nemirovsky, M. C. Rechtsman, and M. Segev, Negative radiation pressure and negative effective refractive index via dielectric birefringence, *Opt. Express* **20**, 8907 (2012).
- [27] H. Cardanus, *Artis Magnae, Sive de Regulis Algebraicis Liber Unus* (Nuremberg, 1545).
- [28] M. J. Weber, *Handbook of Optical Materials* (CRC Press, Boca Raton, FL, 2003).
- [29] M. L. Gorodetsky, A. A. Savchenkov, and V. S. Ilchenko, Ultimate Q of optical microsphere resonators, *Opt. Lett.* **21**, 453 (1996).
- [30] L. D. Landau and E. M. Lifshitz, *Electrodynamics of Continuous Media* (Pergamon Press, New York, 1960).
- [31] R. W. Boyd, *Nonlinear Optics* (Academic Press, New York, 2008).
- [32] W. Cai and V. M. ShalaeV, *Optical Metamaterials* (Springer, Berlin, 2010).
- [33] R. Descartes, *Discours de la méthode plus la Dioptrique, Discours de la méthode plus la Dioptrique, les Météores et la Géométrie* (Jan Maire, Leiden, 1637), pp. 376–493.